Journal of Physics:
Conference Series

PAPER • **OPEN ACCESS**

Conformal mapping as an analytical tool for hydrodynamic analysis in corrugated pipe flows

To cite this article: Mohamed Kh Hassanin *et al* 2025 *J. Phys.: Conf. Ser.* **3058** 012015

Conformal mapping as an analytical tool for hydrodynamic analysis in corrugated pipe flows

Mohamed Kh Hassanin[1], Abdelhamid Attia[2], Amr M Abdelrazek[1].

[1]Department of Engineering Mathematics and Physics, Faculty of Engineering, Alexandria, 21544, Alexandria, Egypt.
[2]Mechanical Engineering Department, Faculty of Engineering, Alexandria, 21544, Alexandria, Egypt.
E-mail: mohamed.khairy@alexu.edu.eg

Abstract. An investigation of steady laminar flow in transversely corrugated conduits is presented, with the velocity distribution and frictional resistance being characterized for the fully developed region, while the incremental pressure drop, and hydrodynamic entrance length are examined for the developing region. The velocity field throughout both flow regimes is modeled using an innovative analytical approach based on epitrochoidal coordinate transformations. It is demonstrated that in fully developed flow, the Fanning friction factor is reduced with either an increase in corrugation count at fixed amplitude or with larger corrugation amplitude at fixed wave number. Conversely, in the developing flow region, both the incremental pressure drop, and entrance length are found to increase with greater corrugation amplitude or number of boundary waves. These findings are shown to provide valuable insights for the optimization of corrugated conduit designs in applications where entrance effects are significant, such as in compact heat exchangers and microfluidic systems.

Key words: Conformal mapping, Friction coefficient, Epitrochoid mapping, incremental pressure drop, hydrodynamic entry length.

1. Introduction

While laminar flow in circular conduits is well-characterized and widely utilized in thermal systems, non-circular geometries remain understudied despite their engineering relevance. Nevertheless, for the development of compact heat exchangers and other similar applications, having analytical and experimental data regarding laminar forced convection in non-circular ducts is crucial [1]. A variety of industrial applications, such as compact heat exchangers, gas-cooled nuclear reactors, gas turbines, extruders, oil/gas drilling wells, and more, involve the use of flow through non-circular tubes [2]. Numerous researchers have conducted numerical simulations to explore the flow characteristics, pressure drop, and incremental pressure drop in both smooth and corrugated tubes [3]. These studies often employ advanced computational techniques, such as Finite Difference Method (FDM), Finite Element Method (FEM), Finite Volume Method (FVM), and other particle-based methods, which are critical for understanding fluid dynamics in complex geometries [4]. Through these simulations, significant insights can be gained regarding the behavior of fluids under varying conditions, contributing to improvements in design and operational efficiency across multiple engineering disciplines. One significant factor affecting pressure drop in laminar flow is the geometry of the pipe itself. For instance, when comparing elliptic pipes to circular ones with the same cross-sectional area, the pressure drop for liquefied petroleum gas (LPG) flowing through elliptic pipes was observed to be higher [5]. This suggests that non-circular geometries may lead to increased resistance, which could be crucial

information for engineers designing compact heat exchangers or other devices requiring efficient fluid transport.

Numerical simulations [6] were performed to investigate flow behavior, pressure drop, and heat transfer enhancement in smooth and corrugated tubes. The study explored the impact of different corrugation amplitude on water flow at various Reynolds numbers, with the goal of identifying optimal configurations for improved heat transfer efficiency. An analytical investigation explored the friction coefficient and Nusselt number in transversely corrugated tubes, demonstrating that both parameters decline when the corrugation amplitude increases at a fixed number of corrugations or when the number of corrugations increases while maintaining a constant amplitude [7]. Beyond pressure drop and heat transfer, entrance length is another crucial factor in conduit design. Numerous studies have aimed to determine the entrance length for both circular and non-circular conduits. One particular study examined conduits with various cross-sectional shapes, such as circular, triangular, square, and hexagonal, to estimate their entrance lengths [8]. The findings indicated that the entrance length is highly influenced by the conduit's geometry, with non-circular shapes generally requiring longer development lengths than circular ones.

This research investigates the flow of Newtonian fluids through straight, transversely corrugated pipes under steady, incompressible laminar flow conditions. The velocity distribution and frictional resistance are analyzed in the fully developed region, while the incremental pressure drop, and hydrodynamic entrance length are evaluated in the developing region. Emphasis is placed on understanding how pipe wall corrugations—including their amplitude and number—affect these flow characteristics. By distinguishing between developed and developing flow regimes, the study reveals how geometric modifications influence pressure losses. The findings offer insights applicable to the design of heat exchangers, microfluidic systems, and other engineering devices where wall shaping is used to manipulate fluid flow.

2. Analytical solution

The flow is assumed to be steady, fully developed, and laminar in both the thermal and hydrodynamic senses. The constitutive parameters are considered independent of temperature, leading to constant fluid properties. This study examines the case of a constant heat flux at the wall. It is further assumed that Fourier's law of heat conduction applies and that neither internal energy nor thermal conductivity is explicitly affected by the velocity gradient or other kinematic variables. Under these assumptions, the hydrodynamic and thermal problems are completely independent. The velocity field solution is first presented, followed by the solution to the thermal problem, which is the primary focus of this report.

2.1 Analytical solution for the velocity field.

The analysis focuses on the Poiseuille flow of a Newtonian fluid through a tube with an average outer radius R. Due to the symmetry of the system, the velocity field is confined to a single direction $v = [0, 0, w(x, y)]$. As a result, the Navier–Stokes equations simplify significantly.

$$\frac{\partial p}{\partial x} = 0, \qquad \frac{\partial p}{\partial y} = 0, \quad \frac{\partial p}{\partial z} = \mu\left(\frac{\partial^2 w}{\partial x^2} + \frac{\partial^2 w}{\partial y^2}\right) \tag{1}$$

The flow domain is transformed into an area within the unit circle using the epitrochoid conformal mapping [9].

$$\zeta = x + iy = \xi + \frac{\varepsilon \xi^{n+1}}{R^n} \tag{2}$$

for $n \geq 1$ and ε as constants, the transformed domain ξ is defined as follows:

$$\xi = re^{i\theta}, \qquad 0 \leq r \leq R \qquad and - \pi \leq \theta \leq \pi$$

Or, equivalently, in terms of Cartesian coordinates x and y,

$$x = rcos(\theta) + \varepsilon \frac{r^{n+1}}{R^n} cos\big((n+1)\theta\big) \tag{3}$$

$$y = rsin(\theta) + \varepsilon \frac{r^{n+1}}{R^n} sin\big((n+1)\theta\big) \tag{4}$$

The condition for this mapping to be conformal is $|\varepsilon|(n+1) < 1$. The number of the corrugation is given by $\frac{2\pi}{n}$ due to the presence of n peaks, while ε represents the amplitude, as the outer radius varies between $1 \pm \varepsilon$. **Figure 1** illustrates two examples of corrugated geometries one with $n = 3\ and\ \varepsilon = 0.24, and\ another\ with\ n = 6\ and\ \varepsilon = 0.12$.

(a) (b)

Figure 1. Flow domain for different geometric configurations: (a) n = 3, ε = 0.24; (b) n = 6, ε = 0.12.

After applying the epitrochoid mapping, the transformation Jacobian is:

$$J = r\left(1 + \varepsilon^2 (n+1)^2 \frac{r^{2n}}{R^{2n}} + 2\,\varepsilon\,(n+1)\,\frac{r^n}{R^n}\,cos(n\,\theta)\right) \tag{5}$$

So, equation (1) can be written as,

$$\frac{1}{J}\left(r\frac{\partial^2 w}{\partial r^2} + \frac{\partial w}{\partial r} + \frac{1}{r}\frac{\partial^2 w}{\partial \theta^2}\right) = \frac{1}{\mu}\frac{\partial p}{\partial z} \tag{6}$$

with boundary conditions of;

$$w(0,\theta) \neq \infty, w(R,\theta) = 0, \frac{\partial w(r,0)}{\partial \theta} = \frac{\partial w\left(r,\frac{2\pi}{n}\right)}{\partial \theta} = 0 \tag{7}$$

Equation (6) is a non-homogeneous PDE, its homogeneous solution is,

$$\begin{aligned} w_{hom} &= \left(c_1\, ln\left(\frac{r}{R}\right) + c_2\right)(a_1 t + b_1) \\ &+ (C_1 r^m + C_2 r^{-m})(a_2\, cos(m\,t) + b_2\, sin(m\,t)), \text{for m } 1,2,3,. \end{aligned} \tag{8}$$

The solution for the particular integral can be expressed as:

$$w_{PI} = \frac{R^2}{4}\frac{1}{\mu}\frac{\partial p}{\partial z}\left(\left(\frac{r}{R}\right)^2 + \varepsilon^2\left(\frac{r}{R}\right)^{2n+2} + 2\varepsilon\left(\frac{r}{R}\right)^{n+2} cos(n\,\theta)\right) \tag{9}$$

So, the general solution is as follows:

$$\begin{aligned} w = \left(c_1\, ln\left(\frac{r}{R}\right) + c_2\right)(a_1 t + b_1) + (C_1 r^m + C_2 r^{-m})(a_2\, cos(m\,\theta) + b_2\, sin(m\,\theta)) \\ + \frac{R^2}{4}\frac{1}{\mu}\frac{\partial p}{\partial z}\left(\left(\frac{r}{R}\right)^2 + \varepsilon^2\left(\frac{r}{R}\right)^{2n+2} + 2\varepsilon\left(\frac{r}{R}\right)^{n+2} \cos(n\theta)\right) \end{aligned} \tag{10}$$

Applying the following condition, $w_\theta(\mathrm{r}, 0) = 0$, therefore $\mathrm{a}_1 = \mathrm{b}_2 = 0$

$$\begin{aligned} w = c_1\, ln\left(\frac{r}{R}\right) + c_2 + (\mathrm{A}\, r^m + \mathrm{B}\, r^{-m}) cos(m\,\theta) \\ + \frac{R^2}{4}\frac{1}{\mu}\frac{\partial p}{\partial z}\left(\left(\frac{r}{R}\right)^2 + \varepsilon^2\left(\frac{r}{R}\right)^{2n+2} + 2\varepsilon\left(\frac{r}{R}\right)^{n+2} \cos(n\,\theta)\right) \end{aligned} \tag{11}$$

Because of the conditions, $w(0, \theta) \neq \infty$, it is found that $\mathrm{c}_1 = \mathrm{B} = 0$.

$$w = c_2 + \mathrm{A}\, r^m cos(m\,\theta) + \frac{R^2}{4}\frac{1}{\mu}\frac{\partial p}{\partial z}\left(\left(\frac{r}{R}\right)^2 + \varepsilon^2\left(\frac{r}{R}\right)^{2n+2} + 2\varepsilon\left(\frac{r}{R}\right)^{n+2} \cos(n\,\theta)\right) \tag{12}$$

The boundary condition, $w_\theta\left(\mathrm{r}, \frac{2\pi}{\mathrm{n}}\right) = 0$, results in $\mathrm{m} = \frac{\mathrm{in}}{2}$, *where* $i = \pm 1, \pm 2, \ldots$

$$w = \mathrm{c}_2 + \sum_{i=1}^{\infty} A_i r^{\frac{i\,n}{2}} cos\left(\frac{i\,n}{2}\theta\right) + \frac{R^2}{4\mu}\frac{\partial p}{\partial z}\left(\left(\frac{r}{R}\right)^2 + \varepsilon^2\left(\frac{r}{R}\right)^{2n+2} + 2\varepsilon\left(\frac{r}{R}\right)^{n+2} cos\,(n\,\theta)\right) \tag{13}$$

The last boundary condition $w(R, \theta) = 0$, results in $\mathrm{c}_2 = -\frac{R^2}{4\mu}\frac{\partial p}{\partial z}(1 + \varepsilon^2)$ *and* $A_2 = -\frac{R^2}{4\mu}\frac{\partial p}{\partial z}(2\varepsilon)$ *while* $A_i = 0$ *for* $i \neq 2$.

It is found that the final velocity is:

$$w = -\frac{R^2}{4\mu}\frac{\partial p}{\partial z}\left(1 - \left(\frac{r}{R}\right)^2 + \varepsilon^2\left(1 - \left(\frac{r}{R}\right)^{2n+2}\right) + 2\varepsilon\left(\frac{r}{R}\right)^n\left(1 - \left(\frac{r}{R}\right)^2\right)\cos(n\,\theta)\right) \tag{14}$$

The flowrate can be determined using the following integral,

$$Q = n\int_0^{\frac{2\pi}{n}}\int_0^R w(r, \theta) J dr d\theta \tag{15}$$

$$Q = -\frac{\pi R^4}{4\mu}\frac{\partial p}{\partial z}\left(1 + 4\varepsilon^2 + \varepsilon^4(1 + n)\right) \tag{16}$$

The area of the pipe is calculated using the following integration $A = n\int_0^{\frac{2\pi}{n}}\int_0^R J dr d\theta$

$$\mathrm{A} = \pi R^2\left(1 + \varepsilon^2(1 + n)\right) \tag{17}$$

Now, the average velocity can be calculated from the following formula $w_{avg} = \frac{Q}{A}$

$$w_{avg} = -\frac{R^2}{4\mu}\frac{\partial p}{\partial z}\frac{\left(1+4\varepsilon^2+\ \varepsilon^4(1+n)\right)}{\left(1+\varepsilon^2(n\ +\ 1)\right)} \tag{18}$$

Since the friction coefficient times the Reynolds number is determined from,

$$fR_e = -\frac{1}{\mu}\frac{\partial p}{\partial z} * \frac{2 * {D_h}^2}{w_{avg}}$$

The wetted perimeter is determined numerically from the following relation for some known wavelength and corrugation number.

$\hat{\mathrm{P}} = R\int_0^{2\pi}\sqrt{1+\varepsilon^2(n+1)^2+2\varepsilon(n+1)cos(n\theta)}dt$. The hydrodynamic diameter is $D_h = \frac{4A}{\hat{\mathrm{P}}}$.

$$fR_e = 8\left(\frac{D_h}{R}\right)^2\frac{\left(1+\varepsilon^2(n\ +\ 1)\right)}{\left(1+4\varepsilon^2+\ \varepsilon^4(1+n)\right)} \tag{19}$$

2.2 The effect of the development of the flow in the entrance on the pressure drop and the length of the full hydrodynamic development.

In the hydrodynamic entrance region, the total pressure drop comprises three components: (1) the momentum change due to flow profile development, (2) the increasing wall shear stress as the boundary layer grows, and (3) the baseline pressure drop equivalent to that in fully developed flow. This combined effect occurs as the flow transitions from its entrance condition to a fully developed velocity profile. Lundgren et al. [10] calculated the pressure in the developing region at any cross section by:

$$\frac{(\mathrm{P_o}-P)}{\frac{1}{2}\rho w_{avg}^2} = f\frac{z}{D_h} + K_p \tag{20}$$

where Po, P and K_p are the back pressure, pressure at z and the incremental pressure drop, respectively. It has been demonstrated that the incremental pressure drop can be directly calculated from:

$$K_p = \frac{2}{A}\int_0^{\frac{2\pi}{n}}\int_0^{R} nJ\left(\left(\frac{w(r,\theta)}{w_{avg}}\right)^3 - \left(\frac{w(r,\theta)}{w_{avg}}\right)^2\right)drd\theta\,, \tag{21}$$

where $w(r,t)\ and\ w_{avg}$ are the fully developed velocity profile equation (14) and the average velocity equation (18), respectively. McComas [11] built upon the research conducted by Lundgren et al. [10] to calculate the required duct length for complete flow development. The length is expressed as follows:

$$\frac{L_e}{D_h Re} = \frac{\left(\left(\frac{w_{max}}{w_{avg}}\right)^2 - 1 - K_p\right)}{f.Re}, \tag{22}$$

where $\mathrm{L_e}$, w_{max} are the hydrodynamic entrance length and the maximum velocity, respectively. The maximum velocity can be determined numerically for each case of K at specified wavelengths and a defined number of corrugations.

3. Discussion

The results derived from the analytical solution are presented in this section, with a detailed analysis focused on the friction factor, the incremental pressure drop and the hydrodynamic entry length. Applying epitrochoid mapping, with the condition $|\ \varepsilon\ |\ (n+1) < 1$ to ensure conformality, provides a powerful representation of transversally corrugated geometries with arbitrary amplitudes, and varying

numbers of boundary waves. **Figure 1** illustrates two cases of mapping for n = 3 and n = 6, respectively. In both cases, the values of ε are proximate to their respective critical values, ε_c, from a lower bound. To simulate the influence of boundary roughness, one can employ a mapping with a large n and a very small ε, while ensuring conformal mapping. The application of this approach to roughness simulation in microtubes, along with its implications and effects on fluid flow, is currently under investigation.

Figure 2. illustrates the relationship between the friction factor, f multiplied by the Reynolds number Re and the amplitude ε of corrugation for various values of waviness n for the corrugated pipe with fully developed laminar flow.

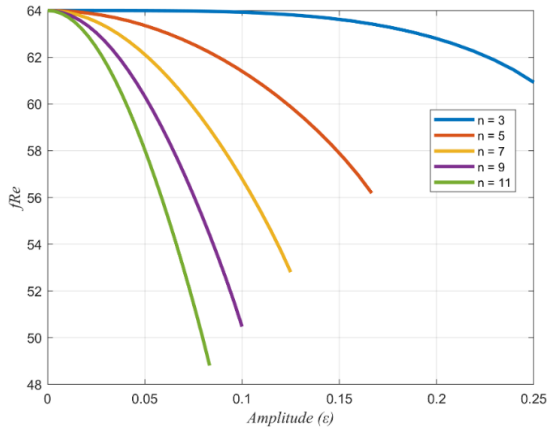

Figure 2. Impact of corrugation amplitude ε and waviness n on the friction coefficient f times Reynolds number Re.

The plots show that as the corrugation amplitude increases, the fRe product decreases for all values of n. Moreover, for a constant ε, a higher waviness typically causes a further decrease in fRe. This decrease becomes more pronounced with larger values of n, providing useful insights for optimizing fluid flow in corrugated tubes, such as those found in heat exchangers or other fluid transport applications.

The correlation between the incremental pressure drop K_p and the corrugation amplitude for different number of corrugations is illustrated in **Figure 3**.

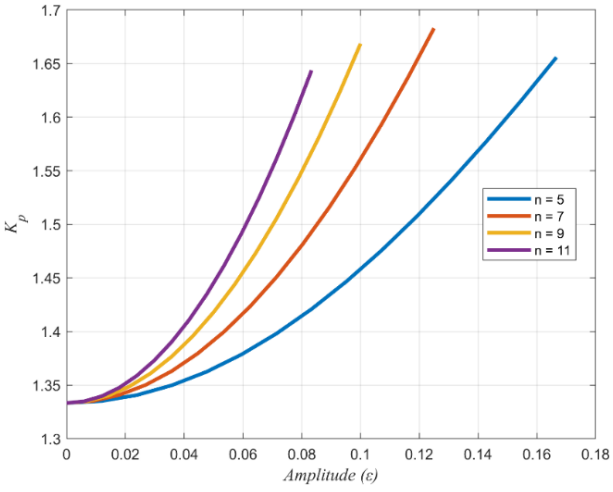

Figure 3. Effect of corrugation amplitude ε and waviness n on the incremental pressure drop K_p.

The results indicate that the incremental pressure drop K_p increases nonlinearly with increasing amplitude for all cases. Additionally, at a given amplitude, a higher number of corrugations n leads to a greater incremental pressure drop. This suggests that increasing the waviness magnifies flow resistance, which is a crucial consideration in the design and optimization of corrugated pipes for heat transfer and fluid flow applications.

The impact of corrugation amplitude on the dimensionless entrance length $\frac{L_e}{D_h Re}$ is shown in **Figure 4** for various number of corrugations under fully developed laminar flow.

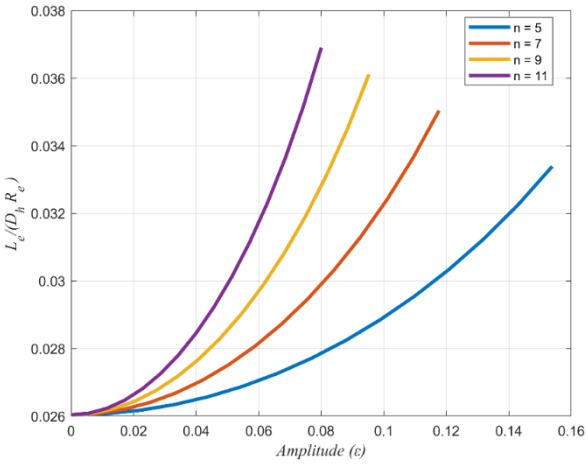

Figure 4. Impact of corrugation amplitude ε and waviness n on the dimensionless entrance length $\frac{L_e}{D_h Re}$

.

The figure demonstrates a nonlinear increase in the loss coefficient $\frac{L_e}{D_h Re}$ with growing amplitude ε for various numbers of corrugations n. At any fixed amplitude, higher values of n result in greater loss coefficients, indicating increased flow resistance. This trend underscores the significant impact of both amplitude and corrugation number on flow dynamics in corrugated pipes.

4. Conclusion

This study analytically examines the impact of corrugation amplitude and the number of boundary waves on frictional resistance, incremental pressure drops, and entrance length in transversely corrugated conduits. The innovative use of epitrochoidal coordinate transformations provides a robust analytical framework for understanding fluid flow in complex geometries. The results indicate that increasing the number of corrugations decreases the friction factor while increasing both the incremental pressure drop and entrance length. These findings are crucial for optimizing the design of corrugated pipes in various engineering applications, particularly in compact heat exchangers and other systems requiring efficient fluid transport. Future research could explore the application of this methodology to different types of fluids and more complex pipe geometries, further expanding the scope of analytical hydraulic calculations in fluid dynamics.

References

[1] Antonini Alves T, Ramos R and Maia C R M 2015 Laminar flow inside circular sector ducts *Ciencia y Engenharia/ Science and Engineering Journal* **24** 65-74
[2] Elsamni O A, Abbasy A A and El-Masry O A 2019 Developing laminar flow in curved semi-circular ducts *Alexandria Engineering Journal* **58** 1-8
[3] bin Ismail H and Nguyen M Q 2023 A Comparative Analysis of Efficiency in Fluid Dynamic Devices: Experimental and Computational Approaches *Quarterly Journal of Emerging Technologies and Innovations* **8** 85-102

[4] Sobieski W and Šarler B 2023 Numerical methods in fluid mechanics–an overview *Technical Sciences/University of Warmia and Mazury in Olsztyn*
[5] Lasode O, Popoola O and Prasad B 2014 Pressure drop in liquefied petroleum gas laminar flow in cylindrical elliptic pipes *Brazilian Journal of Petroleum and Gas* **7**
[6] Al-Obaidi A R 2019 Investigation of fluid field analysis, characteristics of pressure drop and improvement of heat transfer in three-dimensional circular corrugated pipes *Journal of Energy Storage* **26** 101012
[7] Talay Akyildiz F and Siginer D A 2019 Laminar Forced Convection in Transversely Corrugated Microtubes *Journal of Heat Transfer* **141** 031702
[8] Tongpun P, Bumrungthaichaichan E and Wattananusorn S 2014 Investigation of entrance length in circular and noncircular conduits by Computational Fluid Dynamics simulation.
[9] Muskhelishvili N I 1953 *Some basic problems of the mathematical theory of elasticity* vol 15: Noordhoff Groningen)
[10] Lundgren T, Sparrow E and Starr J 1964 Pressure drop due to the entrance region in ducts of arbitrary cross section
[11] McComas S 1967 Hydrodynamic entrance lengths for ducts of arbitrary cross section

Nomenclature

x, y, z	Coordinates in the flow domain (m)	ε	Amplitude of the corrugations
r, θ, z	Coordinates in the transformed domain (m)	J	Jacobian
R	Average radius of the outer surface	ζ, ξ	Complex functions in the flow domain and mapped computational domain, respectively
w	Axial velocity	μ	Viscosity
p	Pressure	w	Axial velocity
n	Number of corrugations	Q	Flow rate
D_h	Hydraulic diameter	K_p	Incremental pressure drops.
f, R_e	Friction factor and Reynolds number.	L_e	Hydrodynamic entrance length.